

Experimental study on surface wave modifications by different ice covers

Sabrina M. Parra^{a,b,*}, Dharma K.K. Sree^{c,d}, David Wang^e, Erick Rogers^e, Jung H. Lee^f,
Clarence O. Collins III^g, Adrian Wing-Keung Law^{c,d}, Alexander V. Babanin^f

^a American Society for Engineering Education with the US Naval Research Laboratory, Stennis Space Center, MS 39529, USA

^b Now at Johns Hopkins University, Applied Physics Laboratory, Laurel, MD 20723, USA

^c Environmental Process Modelling Centre (EPMC), Nanyang Environment and Water Research Institute (NEWRI), Nanyang Technological University, CleanTech One, 637141, Singapore

^d School of Civil and Environmental Engineering, Nanyang Technological University, 50 Nanyang Avenue, 639798, Singapore

^e Oceanography Division, US Naval Research Laboratory, Stennis Space Center, MS, 39529, USA

^f University of Melbourne, Parkville, Victoria 3010, Australia

^g Field Research Facility, Coastal And Hydraulics Laboratory, US Army Corps of Engineers, Kitty Hawk, North Carolina, USA



ARTICLE INFO

Keywords:

Wave-ice interactions
Experimental study
Grease ice
Ice floes
Sheet ice
Phase speed
Wave amplitude attenuation
Young's modulus

ABSTRACT

A laboratory experimental study conducted in a freshwater wave flume installed in a refrigerated room characterized the modifications of wave propagation along on-site manufactured ice covers. Monochromatic surface waves of various amplitudes and frequencies were generated and propagated through three types of ice covers: sheet ice, broken ice floes, and grease ice. This study characterized the spatial evolutions of wave height attenuation and phase speed changes. Wave phase speed increased significantly in sheet ice relative to open water values while no significant changes in phase speed were present with other ice covers. The modifications by sheet ice are consistent with thin plate model predictions based on the elasticity of ice, using measured mechanical properties of sheet ice. Attenuation was strongest for shorter waves in sheet ice followed by grease ice and ice floes. Attenuation under grease ice is shown to be related to the surface wave orbital velocity, similar to dissipation by bottom friction and swell dissipation. The attenuation coefficient of grease ice normalized by wavenumber is proportional to wave steepness with a coefficient varying with ice properties. This laboratory experimental study examined and characterized wave dispersion and attenuation under these different ice properties and wave characteristics, which could be useful in understanding and modeling wave-ice interaction processes in open waters.

1. Introduction

The dynamic region at the edge of the ice-covered sea is known as the Marginal Ice Zone (MIZ), and spans from the open water to the interior continuous ice cover (Wadhams et al., 1988). The MIZ is increasingly important because of an accelerated ice retreat caused by climate changes, which leads to larger areas of open water where waves can develop (Comiso et al., 2008; Thomson and Rogers, 2014). The MIZ consist of mixed ice, from frazil ice to ice floes and larger sheets that cover the edge zone, the transition zone, and the interior zone, respectively (Squire and Moore, 1980; Wadhams et al., 1988; Webber, 1987). The extent of the MIZ depends on the wave and ice conditions, where stronger wave action in the open ocean expands the length of the MIZ relative to calmer wave conditions. Wave-ice interactions in the MIZ are complex. Frazil ice is a slurry of newly formed ice crystals that

aggregate near the water surface and it is often referred to as grease ice when it clusters together. Ice evolves from grease to pancake ice under the influence of waves. Waves travel from the open water to the ice interior through a range of ice types, with smaller pancake or frazil ice on the outside that transition to larger ice floes or pancakes and finally to large ice floes and solid ice in the interior (Squire, 2007; Squire et al., 1995). Ice floes are broken fragments of the solid sheet ice and can range between a few meters to hundreds of meters in diameter. Under calm water conditions with low temperatures, frazil ice becomes sheet ice.

Wave-forecast models have to be modified to account for the presence of ice. In deep water without ice, the evolution of wind-generated ocean waves can be described by the radiative transfer equation (RTE, e.g., Komen et al., 1994; Young, 1999):

* Corresponding author at: Applied Physics Laboratory, Johns Hopkins University, Laurel, Maryland 20723, USA.

E-mail address: Sabrina.Parra@jhuapl.edu (S.M. Parra).

<https://doi.org/10.1016/j.coldregions.2020.103042>

Received 11 April 2019; Received in revised form 3 March 2020; Accepted 13 March 2020

Available online 16 March 2020

0165-232X/ © 2020 Published by Elsevier B.V.

$$\frac{dN}{dt} = \frac{S_{in} + S_{swl} + S_{ds} + S_{nl} + \dots}{\omega} \quad (1)$$

where $N(k, \theta, x, t) = F(k, \theta, x, t)/\omega$ is the wave action density spectrum, $F(k, \theta, x, t)$ is the two-dimensional wavenumber spectrum, ω is the intrinsic (radian) frequency, k is the wavenumber, and

θ is the direction of wave energy propagation. The intrinsic frequency is related to the wavenumber through the dispersion relation,

$$\omega^2 = gk \tanh(kH) \quad (2)$$

where g is gravitational acceleration and H is the water depth. The RTE (Eq. (1)) represents different physical processes changing the wave energy on the right-hand side, including the wind input term S_{in} , wave breaking term S_{ds} , nonlinear wave-wave interaction S_{nl} , and swell decay S_{swl} , among others (Cavaleri et al., 2007; Holthuijsen, 2007). Dynamics of the wave-interactions bring changes of the RTE both on the right-hand side because of extra dissipation, and on the left-hand side, because of changes in the dispersion relation (Eq. (2)) as in Collins et al. (2016), and hence wave group velocity changes.

To improve understanding and modeling of wave-ice interactions inside the MIZ, field experimental studies of wave-ice interaction under various wave and ice conditions were carried out (Collins et al., 2015; Frankenstein et al., 2001; Marchenko et al., 2017; Meylan et al., 2014; Rabault et al., 2017; Rogers et al., 2016; Sutherland and Rabault, 2016; Wadhams et al., 1988). In general, their results show that wave amplitude attenuations increased with increasing wave frequency, even though there is significant data scatter. Due to the high cost to conduct field experiments in unpredictable environmental conditions, experiment of wave-ice interactions under controlled ice and wave conditions in laboratories is a practical and necessary alternative. A few experimental studies on wave-ice interaction have used on-site manufactured ice covers in temperature-controlled rooms. Experiments using grease ice (Martin and Kauffman, 1981; Newyear and Martin, 1999; Newyear and Martin, 1997) and grease-pancake ice (Wang and Shen, 2010) found wave damping within ice fields. Newyear and Martin (1997) measured an increase in wavelength of up to 30% within the grease ice as compared to open water. Zhao and Shen (2015) compared wave propagation into frazil/pancake, pancake, and fragmented ice cover, with the largest wave attenuations observed under frazil/pancake ice and smallest with the fragmented ice cover (floes). However, few studies have quantified the mechanical properties of the ice; instead, material properties were inferred through inverse calculations in most cases. A summary of wave-ice studies and corresponding details for selected experiments is listed in Table 1.

Although laboratory experiments are invaluable in furthering our understanding of wave-ice interactions under controllable and repeatable wave and ice conditions, no temperature-controlled facility can replicate field sizes of ice and wave (Squire, 2020). There is a large discrepancy of wave attenuation results between field and laboratory experiments. Scaling parameters based on wave dynamics and ice properties to reconcile results from both field observations and laboratory experiments is still an ongoing and challenging task (Yu et al.,

2019).

This study investigates wave-ice interactions and aims to parameterize the changes in wave dispersion and dissipation in terms of wavelength, wave particle motions, and ice types. In the present study, we conducted laboratory experiments to characterize the modification of wave propagation under three types of ice covers: sheet ice, ice floes, and grease ice (Fig. 1). These represented a wide range of ice cover characteristics from long sheets of solid ice to viscous greasy ice. Mechanical and physical properties of the ice were quantified. The paper starts with the experimental setup of the ice manufacturing process, with details on the quantification of ice mechanical and physical properties. This is followed by data collection and analysis for the experiments. The results and discussion include an analysis of wave phase speed and attenuation for different wave characteristics and ice covers, a comparison against models, and a scaling of amplitude attenuation. Finally, major findings are summarized in the conclusion section.

2. Experimental setup

The wave experiments were conducted at the Sea-Ice-Wind-Wave Interaction Facility (SIWWI) at the University of Melbourne, where the 14 m long wave flume is housed within a refrigerated room. The $14 \times 0.75 \times 0.6$ m (length x width x depth) flume is made of 12 mm thick transparent glass panels supported with a structural, marine-treated laminated-veneer-lumber wooden framework (Fig. 2). Glass panels allow full optical access throughout the flume length, and wood limits thermal expansion of the frame under a wide range of temperatures and allows the use of saline water in the flume. The present experiment used freshwater.

The flume is equipped on one end with a custom-built rotating-cam type wave maker driven by an electro-mechanical linear actuator that can generate a range of monochromatic waves of up to 2 Hz frequency. Monochromatic waves can range from ~ 0.5 to 2 s periods and up to ~ 3 cm in amplitude (allowing waves up to steepness, ak , of approximately 0.35, where a is wave amplitude and k is wavenumber for open water). At the opposite end of the flume is an adjustable inclined beach made of PVC coil mat backed by stainless steel mesh. The beach is set to an angle of 7° , although it is not reflection-free. The room temperature could be set within a range from approximately -12°C to ambient laboratory temperatures, enabling the growing and melting of ice. The water depth for the present experiments was maintained at 45 cm. The wave frequencies (f) and amplitudes employed for the experiments were $f = 1.5, 1.0, 0.8, 0.5$ Hz, and $a = 1.0, 1.5, 2.0$ cm (Table 2 shows the amplitude and frequency combinations used).

Seven ultrasound (US) sensors were used to record the vertical displacement of the water/ice surface at various locations along the length of the flume (Fig. 2). The sensors (US 325 and ULS 40 D, General Acoustics, Germany) were identical to those used in Sree et al. (2017). They had a vertical resolution of 0.18 mm with a sampling frequency of 50 Hz. Data from the seven sensors was synchronized using a data acquisition system (NI 9215, National Instruments, Texas) and it was

Table 1
Details of published wave-ice laboratory experiments.

Publications	Ice covers	Water	Flume dimension (L x W x D) m
Martin and Kauffman (1981); Newyear and Martin (1999, 1997)	Grease ice	Saltwater 33 psu	$3.5 \times 1 \times 0.5$
Ogasawara et al. (2013)	Frazil/grease, pancake	Saltwater 3.5 psu	$17 \times 0.5 \times 0.8$
Wang and Shen (2010)	Grease-pancake ice	Saltwater 35 psu	$15 \times 3 \times 0.95$
Zhao and Shen (2015)	Frazil/pancake, pancake, floes	Saltwater 34 psu	$15 \times 3 \times 0.95$
Cheng et al. (2019)	Ice floes	Saltwater 3.73, 4.07 psu	$72 \times 10 \times 2.5$
Marchenko et al. (2019)	Ice sheet, and floes	Saltwater 1.6–3.2 psu	$72 \times 10 \times 2.5$
Rabault et al. (2019)	Grease ice	Freshwater	$3.5 \times 0.3 \times 0.5$
Yiew et al. (2019)	Ice sheet and floes, pancake and grease ice	Freshwater	$14 \times 0.75 \times 0.6$
Herein	Grease ice, long sheet ice, and floes	Freshwater	$14 \times 0.75 \times 0.6$



Fig. 1. Types of manufactured ice for the experiments: a) sheet ice, b) ice floes, and c) grease ice.

recorded using the LABVIEW software. During the sheet ice and ice floe experiments, three sensors were positioned over the open water region and the remaining four sensors were located over the ice-covered region as shown in Fig. 2a. For experiments performed with grease ice, two sensors were located over open water and three over the grease ice as shown in Fig. 2b. The sensors were named US1-US7, numbers increasing downstream.

2.1. Ice covers and manufacturing process

As mentioned before, three types of ice covers (Fig. 1) were manufactured in the flume for the present experiment: a) sheet ice, b) ice floes, and c) grease ice. These different ice covers were chosen for this experiment to represent a wide range of ice types common in and near the MIZ. Sheet ice represents a solid and brittle cover with a length much longer than the wavelength, while ice floes represent a similar solid cover but with a length shorter than the wavelength. Grease ice forms near the edge of the MIZ and acts more like a viscous layer. The three ice types would presumably interact with waves in different ways according to their respective properties. A schematic diagram of the sensor locations for the experiments is shown in Fig. 2, with one setup of sensors for sheet ice and ice floes, and another for grease ice. Prior to the wave-ice experiments, open water experiments were done as a benchmark. The relation between wave period and wavelength for the open water case matched well with the linear wave theory, demonstrating the wave measurement setup and synchronization. Ice covers included sheet ice and floes of 0.5 cm thickness, and grease ice covers of

Table 2

Setup of monochromatic wave amplitude (a) and frequency (f) used during the experiments.

	a (cm)		
	1	1.5	2
f (Hz)	1.5	1.5	1.5
	1.0	1.0	1.0
	0.8	0.8	0.8
	0.5	-	-

25% and 60% volume concentrations. The processes employed to create each ice cover are described below.

2.1.1. Long sheet ice

A long (5 m) sheet of ice of 0.5 cm thickness (ranging from 0.3 to 0.7 cm) was fabricated. The sheet ice was created by setting the air temperature inside the freezer to -6 °C for 15 h overnight, starting with near-freezing water temperatures.

2.1.2. Sheet ice material testing: young's modulus

Mechanical properties of ice are important in understanding and modeling wave-ice interactions. One measured mechanical property was the Young's modulus, Y, which represents the stiffness of the ice. Young's modulus was determined by performing a three-point bending test on sheet ice sample strips. Testing was performed with narrow ice

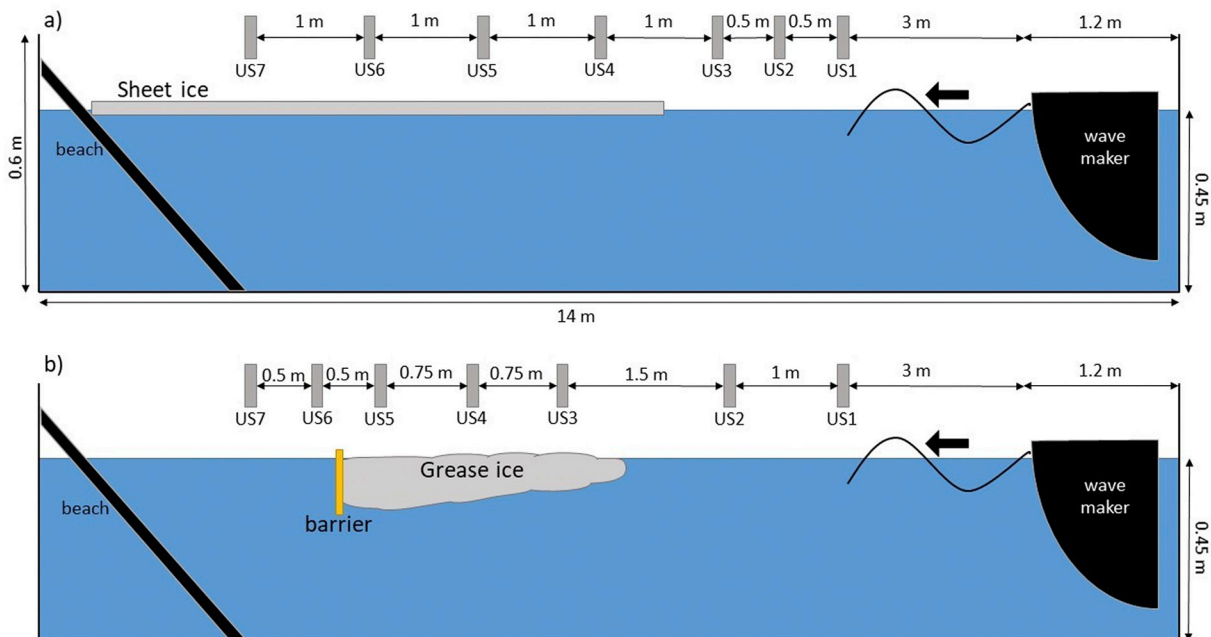


Fig. 2. Flume schematic including experimental setup for a) sheet ice and ice floes, and b) grease ice.

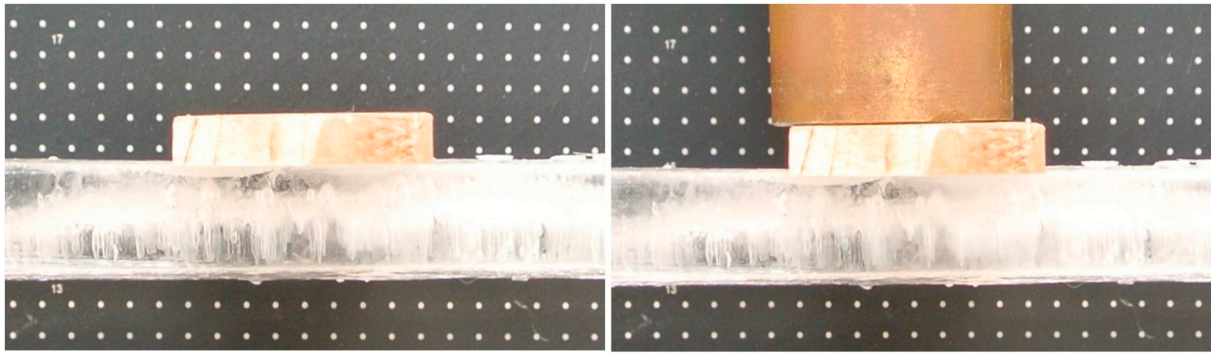


Fig. 3. Ice strip deflections. Ice strips subjected to a three-point bending test, without (left) and with (right) loading. The beige-colored rectangle was a wooden block used to separate and insulate the ice from the weights. The distance between two adjacent dots in the background is 5 mm. The deflection of the ice on the right is 0.8 mm.

Table 3

Young's modulus, Y , along with dimensions and moment of inertia, I , for the tested ice strips. The length, l , width, b , and thickness, h , of each ice strip used to calculate I are described below.

Ice number	b (mm)		h (mm)		l (mm)	$I = \frac{bh^3}{12} \times 10^4 \text{ mm}^4$	Y (GPa)
	(min)	(max)	(min)	(max)			
1	54.4	57.3	12.0	15.3	503	1.19	3.0
2	50/0	50.2	13.5	16.2	503	1.37	2.6
3	46.0	48.4	16.9	16.9	503	1.90	3.1
4	44.5	53.0	14.0	15.0	503	1.24	2.8
5	31.0	31.0	17.0	18.7	503	1.46	2.1
6	17.2	18.6	15.3	19.9	503	0.81	3.1

strips cut out of the sheet ice. All the strips were kept in refrigeration at -8°C and were taken out at the time of the bending test, which on average took 2–5 min to complete at room temperature of $\sim 27^\circ\text{C}$. The warm ambient temperature would result in conservative estimates of Young's modulus, although the average test time was relatively short and likely had a small effect on the ice properties. The strip was held horizontal with the help of supports on either side for a length of 0.503 m, and was loaded at the center with weight (~ 4 cm diameter) applied in 50 g increments until failure. A panel with a marked precision grid was held behind the experimental setup (as shown in Fig. 3) to determine the deflection from each weight increment. The distance between the adjacent markings in the panel was 5 mm. The experiment was recorded using a high-resolution video camera. The videos were converted to images and the pixel distances between the known markings were used to obtain the deflection. Six strips were tested to average over variability in the ice samples, the dimensions of which are provided in Table 3.

Fig. 4a shows the plot for a load F applied at the centre of the beam producing a deflection of δ_{ice} . F varies linearly with δ_{ice} within the

elastic limit, the ice being a brittle material breaks easily once it reaches the yield stress (Hobbs, 1974). The slope of the line is defined by $\frac{dF}{d\delta_{ice}} = \frac{48 Y I}{l^3}$ where $I = \frac{bh^3}{12}$ is the moment of inertia, b is the ice strip width, h is the ice strip thickness, and l is the ice distance between supports (0.503 m). The average ice strip thickness from the six ice strips was 15.9 ± 2.2 mm and the average Young's modulus was 2.8 ± 0.4 GPa (Fig. 4b). The ice thickness used in this test was thicker (1.5 cm) than the ice thickness of our results (0.5 cm); we assumed the calculated Young's modulus is representative of both ice thicknesses. Similar results were obtained for freshwater ice in this wave tank (Dolatshah et al., 2017). Field measurements of Young's modulus in fresh water ice vary from 1.0 GPa to 10.0 GPa depending on the grain type (Gold, 1977). Young's modulus estimates for saltwater ice done by Langleben (1962) showed that it decreases with increasing brine content. In situ measurements of sea ice by Haskell et al. (1996), Marchenko et al. (2017) and Karulina et al. (2019) found elastic modulus values within the same order of magnitude as our findings and decreasing as brine concentrations increased.

2.1.3. Ice floes

Ice floe cover was made from the long sheet ice by gently tapping the ice sheet with a rubber mallet. Care was taken to make the pieces roughly the same size. Ice was broken manually to control floe size. The average area for the floes of thickness 0.5 cm was $97.0 \pm 15.6 \text{ cm}^2$. The location of the sensors for ice floes tests was the same as for sheet ice tests (Fig. 2a).

2.1.4. Grease ice

Grease ice was prepared from ice-free water of $\sim -0.5^\circ\text{C}$ by lowering the temperature of the refrigeration room and running waves for an extended period. The duration of wave action and wave parameters controlled the concentration of grease ice, resulting in the preparation of two volume concentrations: 25% and 60% (estimation of ice concentration is explained in Section 2.1.5). Grease ice of 60% concentration was made with waves of amplitude 1.5 cm and frequency of

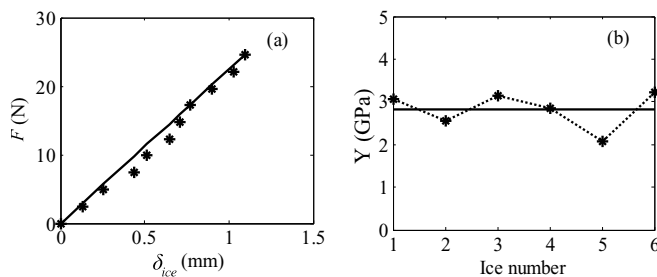


Fig. 4. Determination of Young's modulus, Y . a) Deflection of the ice strips with force applied for strips of average width 47.2 mm and average thickness 16.9 mm (ice #3 in Table 3), and b) Young's modulus for the six strips considered (see Table 3 for details).

1.0 Hz, and by setting the air temperature to $-5.0\text{ }^{\circ}\text{C}$ for 5 h. For the ice of lower concentration (25%), a reduced wave amplitude of 1.0 cm was used while the frequency was maintained at 1.0 Hz, and air temperature set at $-5\text{ }^{\circ}\text{C}$ for 3 h. The thickness of the ice cover increased gradually from the leading ice edge towards the trailing edge, with an average thickness of $\sim 5\text{ cm}$. After each wave experiment, the portions of grease ice that drifted to the open water were moved back to the ice-covered region to maintain a similar ice edge for all experiments. The 25% grease ice concentration is within the 20–40% range used in laboratory experiments by [Martin and Kauffman \(1981\)](#), and it is also consistent with the 25% grease ice concentrations found in the field by [Smedsrud and Skogseth \(2006\)](#).

2.1.5. Grease ice concentration

Physical properties of grease ice concentrations were measured before the test runs in a similar way to [Newyear and Martin \(1997\)](#). The volume concentration was estimated by collecting the ice slurry in a container filled to its brim and measuring the mass. Next, water was removed from the mix and mass of the remaining ice was measured. The volume concentration was calculated as $\frac{m_i}{m_s} \times 100$ where m_i is the ice mass and m_s is the mass of the ice slurry. This test was performed multiple times using ice collected from different sections in the wave flume to improve confidence.

2.2. Measurements of wave phase speed and amplitude attenuation

Each test run began under calm conditions to reduce contamination, resulting in 1–3 min between runs depending on ice and wave conditions. Additionally, temperature control was turned off because the refrigerator fans generated small oscillations on the water surface. The time series of surface wave vertical displacement was recorded in an absolute reference frame at 50 Hz and detrended. Surface wave elevations through the ice covers were represented by measurements of the vertical displacement. A moving average filter was applied to the ice-cover time series data to delineate the wave profiles from the rough surface of ice floes and grease ice. Wave amplitude was calculated as half the wave height, which was obtained as the mean difference between crest and trough defined as the local maxima and minima of the first five fully developed waves ([Fig. 5](#)). This practice allows a determination of wave amplitude from wave elevation acquisition over a relatively short acquisition time to avoid any possible effects from reflected waves in small tanks. Similar techniques of computing wave amplitude have been employed in laboratory experiments by [Sree et al. \(2018, 2017\)](#), and [Yiew et al. \(2019\)](#). [Sutherland et al. \(2017\)](#) and [Rabault et al. \(2019\)](#) computed wave amplitude by integrating wave elevation spectrum around the peak frequency with a narrow integration domain. This spectrum-integration method requires time series of

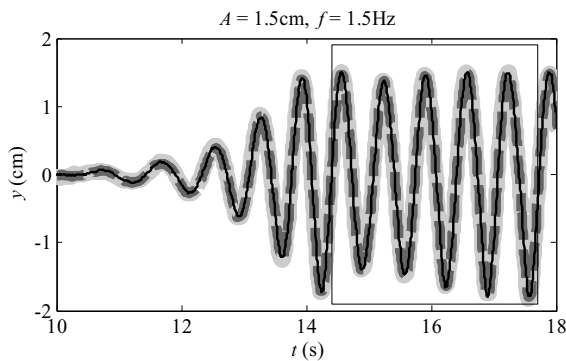


Fig. 5. The time series from US1 (sensor in open water) for waves of 1.5 Hz and 1.5 cm using 0.5 cm thick ice floes with three repetitions (thin solid black, thicker dashed dark gray, and thickest light gray). The five fully developed waves within the rectangle were used for analysis.

wave elevation measurements over a longer duration than our observations.

For multiple peaks within one wave period, only the maximum value among the peaks was selected. Each experiment was repeated three times to check repeatability and only the first five fully developed waves were analyzed to reduce the effects of reflection from the beach.

The open water phase speed applicable to our experimental results was calculated as $c_0 = 2\pi f/k_0$, using

$$(2\pi f)^2 = gk_0 \tanh(k_0 d) \quad (3)$$

where k_0 is the open-water wavenumber, and d is the flume water depth. The measured phase speed, c , within the ice cover was estimated using the sensor vertical displacement time series from the first two sensors within the ice. Phase speed was calculated as the distance between the two sensors divided by the time taken for a wave crest to travel ([Sree et al., 2018; Sree et al., 2017](#)). The wavenumber within the ice cover, k_r , was then calculated as $c = 2\pi f/k_r$. This methodology is similar to what was presented in [Sutherland and Rabault \(2016\)](#), [Sree et al. \(2018, 2017\)](#), [Yiew et al. \(2019\)](#) and [Rabault et al. \(2019\)](#). Wave amplitude modification was quantified using the wave attenuation coefficient, obtained by fitting the wave amplitude spatial variation between two adjacent wave sensor in an ice-covered field with an exponential curve expressed as ([Newyear and Martin, 1997; Wang and Shen, 2010; Zhao and Shen, 2015](#)):

$$a_{i+1} = a_i e^{-qx} \quad (4)$$

where, a_i and a_{i+1} are the wave amplitudes at sensors i and $i + 1$, x is the distance between the two sensors considered, and q is the attenuation coefficient.

3. Results

The evolution of wave phase speed and amplitudes were calculated from the sensors placed across the flume to observe changes in wave characteristics under four different ice covers: sheet ice and ice floes of 0.5 cm thickness, and 25% and 60% grease ice concentrations.

3.1. Modification of wave dispersion

Modifications of the dispersion relation under different ice covers are shown in [Fig. 6](#). Phase speed data within the ice covers were calculated for incident plane waves of the four frequencies ([Table 4](#)). The phase speed under ice covers of grease ice and ice floes was not significantly changed as it followed the open-water dispersion relation (dashed black line in [Fig. 6a](#)). The dispersion relation under the long sheet ice, however, was significantly modified, where k_r becomes much smaller than the open-water wavenumber k_0 as frequency increases ([Fig. 6b](#)). The rather large data scatter of wave dispersion changes by the ice sheet can be partially attributed to the wave sensor's limitation on measurements in heavily attenuated waves.

The modifications of the dispersion relation can be modelled as:

$$\omega^2 = Qgk \tanh(kd), \quad (5)$$

where Q is a non-dimensional parameter for characterizing the effects of ice on the dispersion relation, where $Q = 1$ for ice-free open-water conditions. The dispersion relation is derived from the boundary conditions that require kinematic velocity and dynamic pressure continuity at the interface of waves and ice. The dynamic pressure of ice consists of inertial and elastic responses from wave motions ([Meylan et al., 2018](#)). By neglecting the elastic response, the mass loading model (ML) treats ice cover as added mass at the ice-water interface:

$$Q = 1 - (M\omega)^2, \quad (6)$$

where $M = (\rho_{ice}\gamma h/\rho g)^{0.5}$, γ is the volumetric fraction of ice, h is the ice thickness, and the densities of ice and water are ρ_{ice} and ρ , respectively. By only focusing on the elastic response, the pure elastic (PE) model

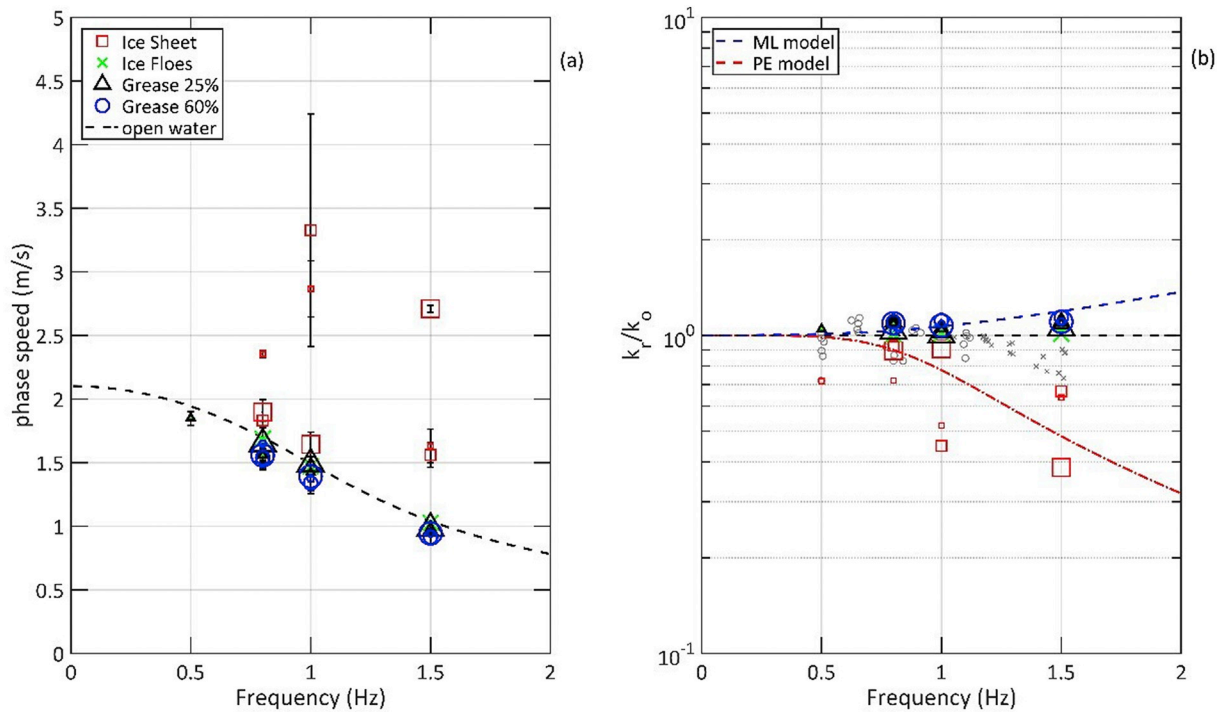


Fig. 6. (a) Phase speed with respect to frequency and ice types. (b) Normalized wavenumber with respect to frequency, compared with the mass loading model (ML; blue dashed line) and pure elastic model (PE; red dashed line). Symbols are the same in both plots: sheet ice (red squares), ice floes (green crosses), grease ice of 25% (black triangles) and 60% (blue circles) concentrations, and open water (black dashed line). The three symbol sizes (small, medium, and large) represent the three wave amplitudes of 1, 1.5, and 2 cm, respectively. Gray crosses and circles in (b) are for data from Newyear and Martin (1997) and Wang and Shen (2010), respectively. The error bar represents the standard deviation of repeated test runs from the mean values of each wave condition. (For interpretation of the references to colour in this figure legend, the reader is referred to the web version of this article.)

treats ice cover as an isotropic, homogenous elastic plate and derives:

$$Q = 1 + (Lk)^4, \tag{7}$$

where L is a characteristic length related to ice rigidity and thickness, $L = \left(\frac{Yh^3}{12(1-\nu^2)\rho g} \right)^{1/4}$ (Sakai and Hanai, 2002), and ν is Poisson's ratio for the ice. Here, L is about 0.25 m, derived from $\nu = 0.3$, $Y = 2.8$ GPa, and $h = 0.5$ cm. The ML model is suitable for representing the ice covers made of ice floes with sizes much shorter than the wavelength such that there is no elastic response from the ice floes ($L = 0$). The PE model represents the effects from ice lengths much larger than the wavelength (Collins et al., 2017; Squire, 2007). In this study, the sheet ice thickness of 0.5 cm was used in the PE model. For the ML model, ice thickness of 0.5 cm was used for ice floe and 5.5 cm for grease ice.

Comparison between observed and modelled dispersion relations were examined by the normalized wavenumber k_r/k_o with respect to

frequency for the four ice covers and the two models (Fig. 6b). The ML model predicts a small increase k_r/k_o with increasing frequency, which is generally consistent with data from grease ice and ice floes for incident waves of 0.5, 0.8 and 1 Hz. The PE model predicts that k_r/k_o will decrease from unity at 0.5 Hz to about 0.5 at 1.5 Hz. This trend is consistent with that under the long sheet ice.

3.2. Wave amplitude attenuation

Spatial attenuation of surface waves under ice covers is quantified by the attenuation coefficient, q . Fig. 7 show q with respect to frequency for the four types of ice cover. In general, shorter waves are attenuated the most as q becomes larger at higher wave frequencies. The attenuation coefficients of sheet ice are on average largest although substantially scattered, followed by those of grease ice and ice floes. As

Table 4

Phase speed, c , and amplitude attenuation coefficient, q , for the different ice covers and wave conditions. The missing values in the table represent runs with unreliable values, thus not used in the subsequent analysis.

Wave conditions		Long sheet ice		Ice floes		Grease ice		Grease ice	
		0.5 cm thick		0.5 cm thick		25%		60%	
a (cm)	f (Hz)	c (m/s)	q (1/m)	c (m/s)	q (1/m)	c (m/s)	q (1/m)	c (m/s)	q (1/m)
1	0.5	–	0.20	1.85	0.11	1.85	0.06	–	0.03
	0.8	2.35	1.02	1.57	–	1.56	0.08	1.65	0.09
	1.0	2.87	1.08	1.43	–	1.42	0.16	1.38	0.13
	1.5	1.63	1.22	1.01	0.58	0.96	0.31	0.94	0.65
1.5	0.8	1.83	0.15	1.67	–	1.54	0.10	1.54	0.10
	1.0	3.33	0.99	1.45	0.01	1.47	0.04	1.34	0.06
	1.5	1.56	0.99	1.00	0.31	0.96	0.50	0.91	0.93
2.0	0.8	1.90	0.12	1.69	–	1.65	0.06	1.56	0.12
	1.0	1.64	0.76	1.49	–	1.49	0.12	1.39	0.15
	1.5	2.71	1.00	1.03	0.12	0.98	0.40	0.94	0.86

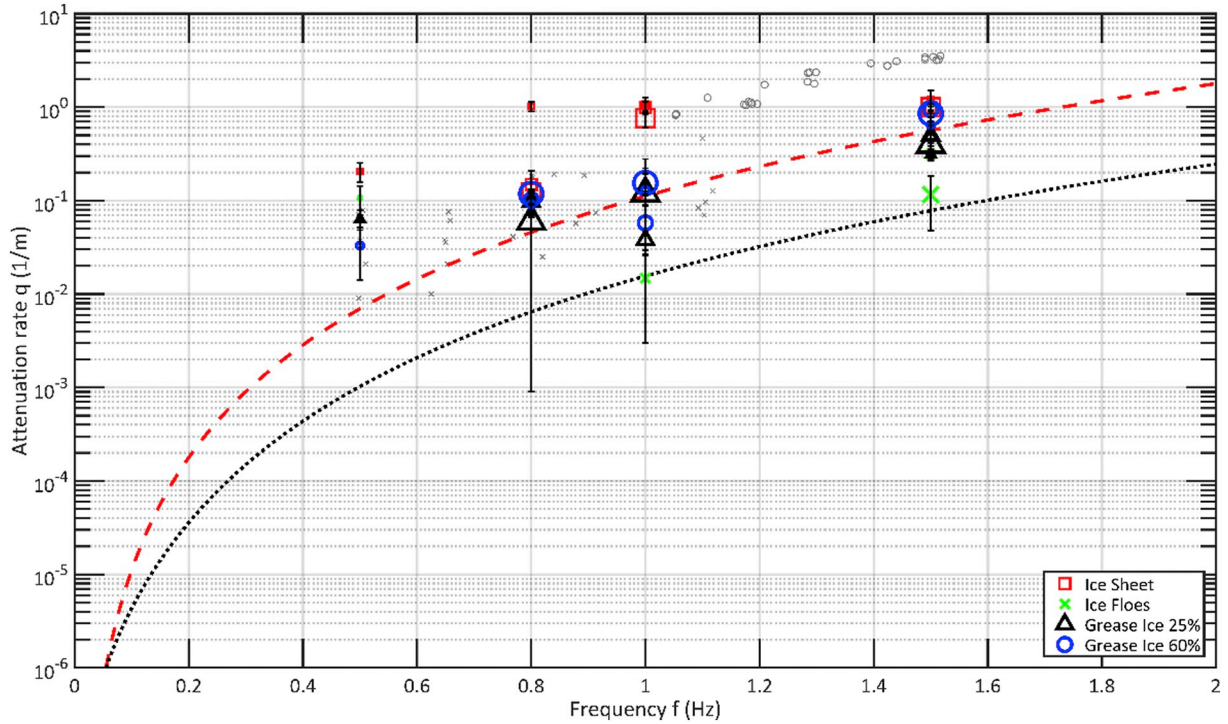


Fig. 7. Wave attenuation coefficients, q , for the four types of ice cover with respect to wave frequency. The three symbol sizes (small, medium, and large) represent three wave amplitudes of 1, 1.5 and 2 cm, respectively. Gray crosses and circles are for data from Newyear and Martin (1997) and Wang and Shen (2010), respectively. The black dotted line is for the binomial functions of Rogers et al. (2018a). The red dashed line is the two-layer model by Sutherland et al. (2019). The error bars represent the standard deviation of repeated test runs from the mean values of each wave condition. Same symbol convention as in Fig. 6. (For interpretation of the references to colour in this figure legend, the reader is referred to the web version of this article.)

an example, the averaged q of 1 Hz waves are about 1.00, 0.10, and 0.01 for ice covers of sheet ice (red squares), grease ice of 60% (blue circles), and ice floe (green cross), respectively. We note that the largest average damping by sheet ice contradicted by results from Yiew et al. (2019) using the same facility. The substantial scattering observed in our results can be attributed to damping caused by sidewall friction and overwash at the leading edge of the ice covers.

Analytically-derived models predict that wave attenuation coefficients follow a power-law dependence of wave frequency as $\alpha \sim f^n$, the coefficient n ranges from 2 to 11 (Meylan et al., 2018). Field data analyses show that the frequency-dependence can be approximated with a binomial function (Rogers et al., 2018a),

$$q_R = c_2 f^2 + c_4 f^4, \quad (8)$$

where c_2 and c_4 are the empirically-fitted coefficients for seven datasets (Table 3 in Rogers et al., 2018a) for wave frequency up to 0.5 Hz and under a wide range of ice types with ice fractions > 0.3 . By using a two-layer structure to represent ice covers, Sutherland et al. (2019) show that the spatial wave decay rate can be modelled as a function of wavenumber expressed as

$$q_S = 0.5\epsilon h k^2, \quad (9)$$

where ϵ is a non-dimensional coefficient with a value less than unity representing the dissipation effect of ice concentration. For comparison with our experiment data, we calculated q_R using coefficient values of $c_2 = 1.06 \times 10^{-3}$ and $c_4 = 2.3 \times 10^{-2}$ from fitting the field measurements of Meylan et al. (2014) and extended the frequency range to 2 Hz. We also computed q_S using $\epsilon = 0.5$ and $h = 0.055$ m, the average ice thickness for grease ice cover. Additionally, attenuation data from the laboratory experiments of Newyear and Martin (1997) and Wang and Shen (2010) are plotted for comparison. Overall, all attenuation coefficients from these experiments, Newyear and Martin (1997), and Wang and Shen (2010) increase with increasing frequency from 0.5 Hz

to 1.6 Hz and are consistent with the trend as predicted by q_R (8) and q_S (9). Although q_S is closer to the laboratory data, the magnitude of attenuation coefficients from the laboratory experiments are larger than q_R and q_S by one to two order of magnitude.

3.3. Phase speed increases in long sheet ice

During the experiments, as waves entered the sheet ice covered region, phase speed increased significantly relative to that in ice-free open water (Fig. 6a). However, no significant increase in phase speed was observed in waves propagated through the smaller ice floes. Both the long sheet ice and fragmented ice floes had the same elasticity and ice thickness, but the difference in length played a key role on the modification of the wave dispersion relation through ice elasticity. For long ice sheets, wave-induced ice bending results in an increase in wave speed through an increase in the wavelength (Boutin et al., 2018; Marchenko and Chumakov, 2017). As floe sizes are reduced, ice floes become more similar to a rigid body in response to wave action and, therefore, wave-induced ice bending diminishes significantly. Changes in the dispersion relation induced by ice elasticity is characterized by a non-dimensional parameter using the relative scales of ice thickness, h , and characteristic length, L (Sakai and Hanai, 2002),

$$\beta = \sqrt{\frac{h}{L}} \ln\left(\frac{l_i}{L}\right), \quad (10)$$

where l_i is the length of the sheet ice or individual ice floes. Sakai and Hanai (2002) showed that a threshold value $\beta = 0.145$ is needed for ice elasticity to start having an impact on the dispersion relation. For $0.15 < \beta < 0.60$, the ratio of effective elasticity to ice elasticity increase from 0 to 1 with increasing β . For floes with $\beta > 0.60$, ice elasticity fully influences changes in the dispersion relation. In our experiments, for an ice sheet of 5 m length and 0.5 cm thickness, $\beta = 0.44$, which is near 0.60. For the smaller ice floes, we estimated

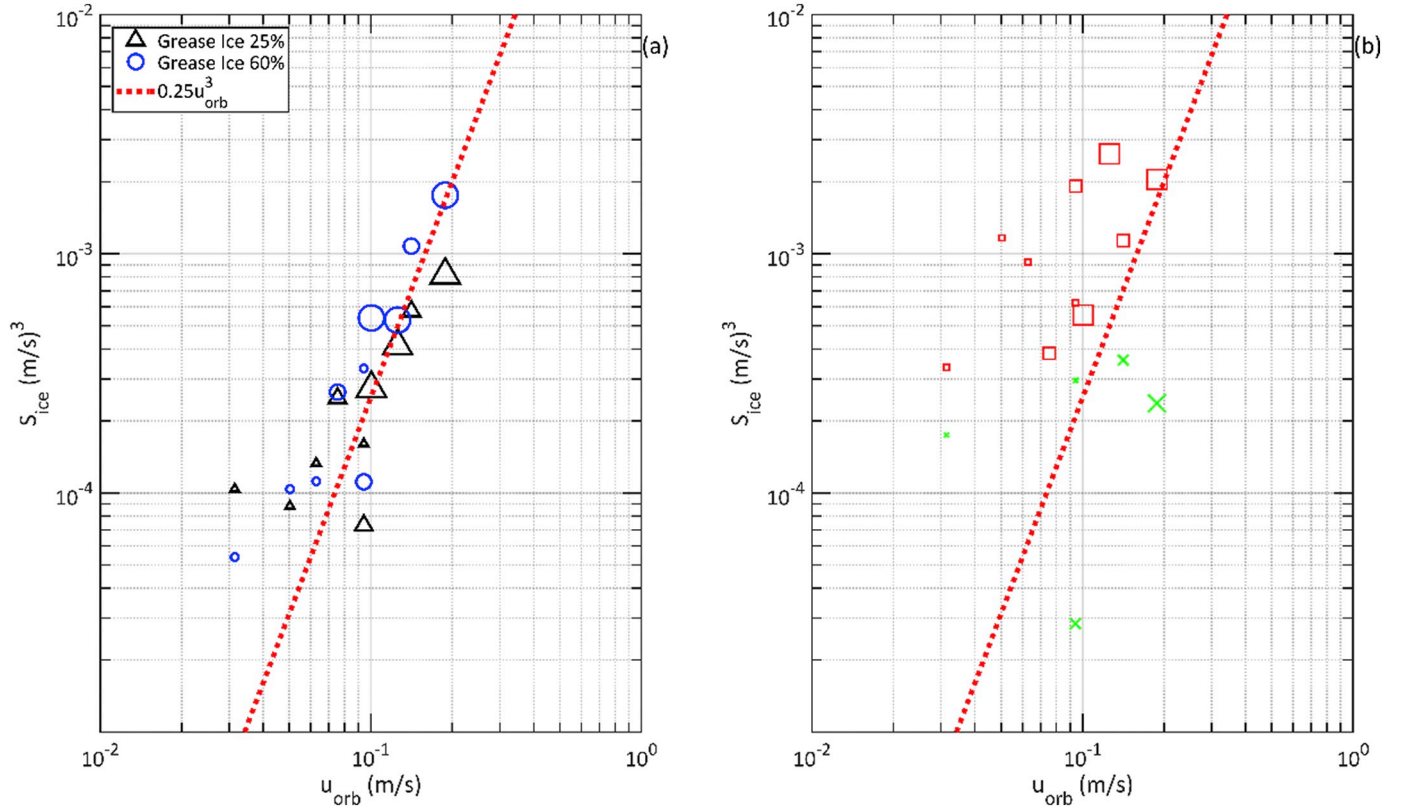


Fig. 8. Wave energy dissipation S_{ice} versus wave orbital velocity at the surface, u_{orb} , for (a) grease ice of two concentrations, and (b) sheet ice and ice floe covers. Same symbol convention as in Fig. 6.

$\beta = -0.10$, which is well below the threshold value of 0.15. Waves propagating through solid sheet ice close to the ice edge likely crack the ice sheets into smaller floes to significantly reduce the ice elasticity effects (Marchenko et al., 2017; Sutherland and Rabault, 2016). This floe size change due to ice cracking could affect the validity of modeling wave propagation near the ice edge using a solid ice sheet.

3.4. Scaling the amplitude attenuation rate with wave properties

Wave energy dissipation by ice S_{ice} can be estimated from the attenuation coefficient, q , as (Rogers et al., 2018b):

$$S_{ice} = -2c_g q E \quad (11)$$

where E is wave energy, and $c_g = 0.5\frac{\omega}{k}$ is group velocity. Here, wave energy is estimated from wave amplitude as $E = \frac{1}{2}g a^2$. The total energy dissipation by ice covers was computed as $S_{ice} = g q c_g a^2$ and plotted against surface wave orbital velocity $u_{orb} = a\omega$ for grease ice, (Fig. 8a) and sheet ice and ice floe covers (Fig. 8b). For grease ice of both concentrations, S_{ice} are correlated well with u_{orb} . The relationship can be approximated by $S_{ice} = 0.25u_{orb}^3$. Similar correlation with u_{orb} was also shown in Voermans et al. (2019). They analyzed collocated field measurements of under-ice turbulence dissipation rate and surface wave energy, showing that the total energy dissipation is related to surface wave orbital speed as $S_{ice} = \alpha u_{orb}^3$, where the non-dimensional coefficient α varies from $\sim 10^{-4}$ to $\sim 10^{-1}$ with increasing ice concentration.

Based on this correlation from both laboratory and field measurements, we can show that the wave amplitude attenuation coefficient normalized by wavenumber is proportional to the wave steepness with a proportionality coefficient related to ice properties as:

$$q/k = 2\alpha(ak). \quad (12)$$

The non-dimensional coefficient α has a mean value of 0.25 from fitting attenuation data of grease ice covers in this experiment and of

$\sim 10^{-4}$ to $\sim 10^{-1}$ from field measurements (Voermans et al., 2019). Dumont et al. (2011) and Herman et al. (2019) derived a very similar expression for amplitude attenuation caused by ice bottom roughness. Dumont et al. (2011) showed $q/k = 2C_d(ak)$, where C_d is a drag coefficient representing ice bottom roughness with values of 0.001, 0.01 and 0.035 from fitting field measurements of wave attenuations.

There is no discernible correlation between wave orbital velocities and S_{ice} from amplitude attenuation of sheet ice and ice floe covers, which are substantially scattered (Fig. 8b). This implies that the dynamic process causing wave attenuation in these ice covers is different from that of grease ice covers. Attenuations for sheet ice and ice floes might have been affected by additional damping from sidewall friction and leading edge overwash. Sidewall derived energy attenuation was estimated using equation 13 in Sutherland et al. (2017), resulting in values that were two orders of magnitude smaller than results in Table 4; this suggests that additional damping could be related to leading edge overwash.

3.5. Measurement of wave properties

Surface wave properties were not directly measured in the presence of the ice covers. Instead, results presented are the vertical motions of the ice covers generated by the propagating waves as measured by the above-ice wave sensors. The vertical displacement at the ice cover surface may not be the same as that of the wave, according to the two-layer system (Zhao and Shen, 2015). Future studies should carefully examine the wave characteristics under the ice as well as the vertical displacement as observed by the sensors.

The observed wave attenuations resulted from multiple factors. Factors responsible for the observed attenuation included overwash, reflection, refraction, scattering, and ice floe collision and rafting (when applicable), in addition to the physical and material properties of the ice covers. Attenuation of the waves could also be attributed to

boundary layer turbulence under the ice covers, which future studies should investigate. Effects from these factors were not separately identified in this study.

3.6. Characterization and quantification of ice properties

This laboratory experiment used real ice to examine the effects of different ice covers on wave properties such as phase speed and attenuation. It is beneficial to use real ice in these studies, as ice rheological properties (such as grease ice concentrations) are difficult to recreate in synthetic versions. In this study we estimated and quantified two different grease ice concentrations, estimated ice parameters such as Young's modulus, thicknesses and average floe area. However, it is difficult to quantify other ice material properties for different types of ice. Therefore, both types of laboratory experiments are useful in the continued understanding of wave-ice interactions.

Another factor to consider is the water salinity. Here we used freshwater ice instead of saltwater ice. Saltwater ice traps brine in small pockets that changes the mechanical and physical properties of the ice, relative to freshwater ice. Freshwater ice is stronger than sea ice, and possesses different grain structures that make it more brittle than sea ice (Timco and O'Brien, 1994).

4. Conclusions

The present study examined and quantified the modification of ice covers on wave properties under different wave conditions and ice covers. The ice covers tested were long sheet ice, broken ice floes, and grease ice of two different concentrations. The long sheet ice cover resulted in increased phase speed, while covers of ice floes and grease ice did not show appreciable changes in phase speed. Wave amplitude attenuations were largest for higher frequencies, with the long sheet ice presenting the largest values, although substantially scattered. This suggests that changes in phase speed and wave amplitude attenuation are associated with the dimensions of the ice, in addition to other ice properties.

Wave amplitudes changed as waves propagated into the different ice covers. Different degrees of wave attenuation were shown for different ice covers, with the largest average attenuation from the long sheet ice cover. Grease ice of both concentrations presented some attenuations, while ice floes showed the least attenuation at most frequencies. Attenuation under grease ice can be related to the surface wave orbital velocity, similar to dissipation by bottom friction and swell dissipation. This was not clearly observed in the long sheet ice cover, where sidewall friction and overwash might have created additional damping.

These results show the effects of wave propagation into different ice covers under the same wave conditions, which allow a direct comparison between them. To connect these small-scale laboratory results to field conditions, proper scaling is necessary using extensive direct measurements of different ice covers with different wave scales. These results expand the collective knowledge of wave-ice interactions, which will be fundamental to understanding the mechanisms involved. Consistency between wave flume experiments and theoretical models with respect to wave frequency-dependence on the modification of wave dispersion and attenuation by ice covers shows that laboratory experiments provide the necessary fundamental knowledge to bridge the gap.

Declaration of Competing Interest

The authors declare that they have no known competing financial interests or personal relationships that could have appeared to influence the work reported in this paper.

Acknowledgement

The authors would like to thank Grant Skidmore and Jason Monty (University of Melbourne, Australia), and Hayley H. Shen (Clarkson University, United States) for the assistance provided throughout this work. The authors gratefully acknowledge the funding provided by the ARC LIEF grant No. LE14010079. Sabrina M. Parra is grateful for funding provided by the U.S. Naval Research Laboratory through an American Society for Engineering Education postdoctoral fellowship. Law W. K. Adrian and Dharma Sree K.K. acknowledge the funding provided by the US Office of Naval Research Global Grant No. N62909-15-1-2069. Alexander V. Babanin acknowledges a grant from the Office of Naval Research No. N00014-17-1-3021.

References

- Boutin, G., Ardhuin, F., Dumont, D., Sévigny, C., Girard-Ardhuin, F., Accensi, M., 2018. Floe size effect on wave-ice interactions: possible effects, implementation in wave model, and evaluation. *J. Geophys. Res. Ocean.* 123, 4779–4805. <https://doi.org/10.1029/2017JC013622>.
- Cavaleri, L., Alves, J.-H.G.M., Ardhuin, F., Babanin, A., Banner, M., Belibassakis, K., Benoit, M., Donelan, M., Groeneweg, J., Herbers, T.H.C., Hwang, P., Janssen, P.A.E.M., Janssen, T., Lavrenov, I.V., Magne, R., Monbaliu, J., Onorato, M., Polnikov, V., Resio, D., Rogers, W.E., Sheremet, A., McKee Smith, J., Tolman, H.L., van Vledder, G., Wolf, J., Young, I., 2007. Wave modelling – the state of the art. *Prog. Oceanogr.* 75, 603–674. <https://doi.org/10.1016/j.poccean.2007.05.005>.
- Cheng, S., Tsarau, A., Evers, K.-U., Shen, H., 2019. Floe size effect on gravity wave propagation through ice covers. *J. Geophys. Res. Ocean.* 124, 320–334. <https://doi.org/10.1029/2018JC014094>.
- Collins, C.O., Rogers, W.E., Marchenko, A., Babanin, A.V., 2015. In situ measurements of an energetic wave event in the Arctic marginal ice zone. *Geophys. Res. Lett.* 42, 1863–1870. <https://doi.org/10.1002/2015GL063063>.
- Collins, C.O., Rogers, W.E., Marchenko, A., 2016. On wave-ice interaction in the Arctic marginal ice zone: Dispersion, attenuation, and ice response. *Nav. Res. Lab. Memo. Rep.* 16–9676 NRL/MR/732.
- Collins, C.O., Rogers, W.E., Lund, B., 2017. An investigation into the dispersion of ocean surface waves in sea ice. *Ocean Dyn.* 67, 263–280. <https://doi.org/10.1007/s10236-016-1021-4>.
- Comiso, J.C., Parkinson, C.L., Gersten, R., Stock, L., 2008. Accelerated decline in the Arctic sea ice cover. *Geophys. Res. Lett.* 35, L01703. <https://doi.org/10.1029/2007GL031972>.
- Dolatshah, A., Nelli, F., Alberello, A., Bruneau, L., Bennets, L.G., Meylan, M.H., Monty, J.P., Toffoli, A., 2017. Wave attenuation due to ice cover: an experimental model in a wave-ice flume. In: ASME 2017 36th International Conference on Ocean, Offshore and Arctic Engineering. American Society of Mechanical Engineers. <https://doi.org/10.1115/OMAE2017-61548>. V008T07A016.
- Dumont, D., Kohout, A., Bertino, L., 2011. A wave-based model for the marginal ice zone including a floe breaking parameterization. *J. Geophys. Res. Ocean.* 116, 1–12. <https://doi.org/10.1029/2010JC006682>.
- Frankenstein, S., Loset, S., Shen, H.H., 2001. Wave-ice interactions in Barents Sea marginal ice zone. *J. Cold Reg. Eng.* 15, 91–102. [https://doi.org/10.1061/\(ASCE\)0887-381X\(2001\)15:2\(91\)](https://doi.org/10.1061/(ASCE)0887-381X(2001)15:2(91)).
- Gold, L.W., 1977. Engineering properties of fresh-water ice. *J. Glaciol.* 19, 197–212. <https://doi.org/10.3189/S0022143000215608>.
- Haskell, T.G., Robinson, W.H., Langhorne, P.J., 1996. Preliminary results from fatigue tests on in situ sea ice beams. *Cold Reg. Sci. Technol.* 24, 167–176. [https://doi.org/10.1016/0165-232X\(95\)00015-4](https://doi.org/10.1016/0165-232X(95)00015-4).
- Herman, A., Cheng, S., Shen, H.H., 2019. Wave energy attenuation in fields of colliding ice floes - part 2: a laboratory case study. *Cryosphere* 13, 2901–2914. <https://doi.org/10.5194/tc-13-2901-2019>.
- Hobbs, P.V., 1974. *Ice Physics*. Clarendon Press, Oxford.
- Holthuijsen, L.H., 2007. *Waves in Oceanic and Coastal Waters*. Cambridge University Press, Cambridge. <https://doi.org/10.1017/CBO9780511618536>.
- Karulina, M., Marchenko, A., Karulin, E., Sodhi, D., Sakharov, A., Chistyakov, P., 2019. Full-scale flexural strength of sea ice and freshwater ice in Spitsbergen Fjords and North-West Barents Sea. *Appl. Ocean Res.* 90. <https://doi.org/10.1016/j.apor.2019.101853>.
- Komen, G.J., Cavaleri, L., Donelan, M., Hasselmann, K., Hasselmann, S., Janssen, P.A.E.M., 1994. *Dynamics and Modelling of Ocean Waves*. Cambridge University Press, Cambridge. <https://doi.org/10.1017/CBO9780511628955>.
- Langbein, M.P., 1962. Young's modulus for sea ice. *Can. J. Phys.* 40, 1–8. <https://doi.org/10.1139/p62-001>.
- Marchenko, A.V., Chumakov, M.M., 2017. Study the surface gravity waves damping in the marginal ice zone of drifting ice in the Barents Sea. *Mod. Approach Promis. Technol. Within Proj. Dev. Oil-and-Gas Fields Russ. Cont. shelf* 4, 94–105.
- Marchenko, A., Rabault, J., Sutherland, G., Collins, C.O., Wadhams, P., Chumakov, M., 2017. Field Observations and Preliminary Investigations of a Wave Event in Solid Drift Ice in the Barents Sea, in: *Proceedings of the International Conference on Port and Ocean Engineering under Arctic Conditions*. (POAC).
- Marchenko, A., Haase, A., Jensen, A., Lishman, B., Rabault, J., Evers, K.-U., Shortt, M., Thiel, T., 2019. Laboratory investigations of the bending rheology of floating saline

- ice, and physical mechanisms of wave damping, in the HSVA ice tank. arXiv Prepr. arXiv 1901.05333.
- Martin, S., Kauffman, P., 1981. A field and laboratory study of wave damping by grease ice. *J. Glaciol.* 27, 283–313.
- Meylan, M.H., Bennetts, L.G., Kohout, A.L., 2014. In situ measurements and analysis of ocean waves in the Antarctic marginal ice zone. *Geophys. Res. Lett.* 41, 5046–5051. <https://doi.org/10.1002/2014GL060809>.
- Meylan, M.H., Bennetts, L.G., Mosig, J.E.M., Rogers, W.E., Doble, M.J., Peter, M.A., 2018. Dispersion relations, power laws, and energy loss for waves in the marginal ice zone. *J. Geophys. Res. Ocean.* 123, 3322–3335. <https://doi.org/10.1002/2018JC013776>.
- Newyear, K., Martin, S., 1997. A comparison of theory and laboratory measurements of wave propagation and attenuation in grease ice. *J. Geophys. Res. Ocean.* 102, 25091–25099. <https://doi.org/10.1029/97JC02091>.
- Newyear, K., Martin, S., 1999. Comparison of laboratory data with a viscous two-layer model of wave propagation in grease ice. *J. Geophys. Res. Ocean.* 104, 7837–7840. <https://doi.org/10.1029/1999JC900002>.
- Ogasawara, T., Ogasawara, A., Sakai, S., 2013. Thermodynamics on Grease-Pancake Ice Growth in a Sea Ice-Wave Tank, in: *The Twenty-Third International Offshore and Polar Engineering Conference*. International Society of Offshore and Polar Engineers.
- Rabault, J., Sutherland, G., Gundersen, O., Jensen, A., 2017. Measurements of wave damping by a grease ice slick in Svalbard using off-the-shelf sensors and open-source electronics. *J. Glaciol.* 63, 372–381. <https://doi.org/10.1017/jog.2017.1>.
- Rabault, J., Sutherland, G., Jensen, A., Christensen, K.H., Marchenko, A., 2019. Experiments on wave propagation in grease ice: combined wave gauges and PIV measurements. *J. Fluid Mech.* 864, 876–898. <https://doi.org/10.1017/jfm.2019.16>.
- Rogers, W.E., Thomson, J., Shen, H.H., Doble, M.J., Wadhams, P., Cheng, S., 2016. Dissipation of wind waves by pancake and frazil ice in the autumn Beaufort Sea. *J. Geophys. Res. Ocean.* 121, 7991–8007. <https://doi.org/10.1002/2016JC012251>.
- Rogers, W.E., Meylan, M.H., Kohout, A.L., 2018a. Frequency distribution of dissipation of energy of ocean waves by sea ice using data from wave array 3 of the ONR Sea State field experiment. *Nav. Res. Lab. Memo. Rep.* 18–9801 NRL/MR/732.
- Rogers, W.E., Posey, P., Li, L., Allard, R., 2018b. Forecasting and hindcasting waves in and near the marginal Ice Zone: Wave modeling and the ONR Sea state field experiment. *Nav. Res. Lab. Memo. Rep.* 18–9786 NRL/MR/732.
- Sakai, S., Hanai, K., 2002. Empirical Formula of Dispersion Relation of Waves in Sea Ice, in: *Ice in the Environment: Proceedings of the 16th IAHR International Symposium on Ice*. International Association of Hydraulic Engineering and Research, Dunedin, New Zealand, pp. 327–335.
- Smetsrud, L.H., Skogseth, R., 2006. Field measurements of Arctic grease ice properties and processes. *Cold Reg. Sci. Technol.* 44, 171–183. <https://doi.org/10.1016/j.coldregions.2005.11.002>.
- Squire, V.A., 2007. Of ocean waves and sea-ice revisited. *Cold Reg. Sci. Technol.* 49, 110–133. <https://doi.org/10.1016/j.coldregions.2007.04.007>.
- Squire, V.A., 2020. Ocean Wave Interactions with Sea Ice: a Reappraisal. *Annu. Rev. Fluid Mech.* 52, 37–60. <https://doi.org/10.1146/annurev-fluid-010719-060301>.
- Squire, V.A., Moore, S.C., 1980. Direct measurement of the attenuation of ocean waves by pack ice [6]. *Nature*. <https://doi.org/10.1038/283365a0>.
- Squire, V.A., Dugan, J.P., Wadhams, P., Rottier, P.J., Liu, A.K., 1995. Of ocean waves and sea ice. *Annu. Rev. Fluid Mech.* 27, 115–168.
- Sree, D.K.K., Law, A.W.-K., Shen, H.H., 2017. An experimental study on the interactions between surface waves and floating viscoelastic covers. *Wave Motion* 70, 195–208. <https://doi.org/10.1016/j.wavemoti.2016.08.003>.
- Sree, D.K.K., Law, A.W.-K., Shen, H.H., 2018. An experimental study on gravity waves through a floating viscoelastic cover. *Cold Reg. Sci. Technol.* 155, 289–299. <https://doi.org/10.1016/j.coldregions.2018.08.013>.
- Sutherland, G., Rabault, J., 2016. Observations of wave dispersion and attenuation in landfast ice. *J. Geophys. Res. Ocean.* 121, 1984–1997. <https://doi.org/10.1002/2015JC011446>.
- Sutherland, G., Halsne, T., Rabault, J., Jensen, A., 2017. The attenuation of monochromatic surface waves due to the presence of an inextensible cover. *Wave Motion* 68, 88–96. <https://doi.org/10.1016/J.WAVEMOTI.2016.09.004>.
- Sutherland, G., Rabault, J., Christensen, K.H., Jensen, A., 2019. A two layer model for wave dissipation in sea ice. *Appl. Ocean Res.* 88, 111–118. <https://doi.org/10.1016/J.APOR.2019.03.023>.
- Thomson, J., Rogers, W.E., 2014. Swell and sea in the emerging Arctic Ocean. *Geophys. Res. Lett.* 41, 3136–3140. <https://doi.org/10.1002/2014GL059983>.
- Timco, G.W., O'Brien, S., 1994. Flexural strength equation for sea ices. *Cold Reg. Sci. Technol.* 22, 285–298. [https://doi.org/10.1016/0165-232X\(94\)90006-X](https://doi.org/10.1016/0165-232X(94)90006-X).
- Voermans, J.J., Babanin, A.V., Thomson, J., Smith, M.M., Shen, H.H., 2019. Wave Attenuation by Sea Ice Turbulence. *Geophys. Res. Lett.* 46, 6796–6803. <https://doi.org/10.1029/2019GL082945>.
- Wadhams, P., Squire, V.A., Goodman, D.J., Cowan, A.M., Moore, S.C., 1988. The attenuation rates of ocean waves in the marginal ice zone. *J. Geophys. Res. Ocean.* 93, 6799–6818. <https://doi.org/10.1029/JC093iC06p06799>.
- Wang, R., Shen, H.H., 2010. Experimental study on surface wave propagating through a grease-pancake ice mixture. *Cold Reg. Sci. Technol.* 61, 90–96. <https://doi.org/10.1016/j.coldregions.2010.01.011>.
- Webber, J.E., 1987. Wave attenuation and wave drift in the marginal ice zone. *J. Phys. Oceanogr.* 17, 2351–2361. [https://doi.org/10.1175/1520-0485\(1987\)017<2351:waawdi>2.0.co;2](https://doi.org/10.1175/1520-0485(1987)017<2351:waawdi>2.0.co;2).
- Yiew, L.J., Parra, S.M., Wang, D., Sree, D.K.K., Babanin, A.V., Law, A.W.K., 2019. Wave attenuation and dispersion due to floating ice covers. *Appl. Ocean Res.* 87, 256–263. <https://doi.org/10.1016/j.apor.2019.04.006>.
- Young, I.R., 1999. *Wind Generated Ocean Waves*. Elsevier, Amsterdam.
- Yu, J., Rogers, W.E., Wang, D.W., 2019. A scaling for wave dispersion relationships in ice-covered waters. *J. Geophys. Res. Ocean.* 124, 8429–8438. <https://doi.org/10.1029/2018JC014870>.
- Zhao, X., Shen, H.H., 2015. Wave propagation in frazil/pancake, pancake, and fragmented ice covers. *Cold Reg. Sci. Technol.* 113, 71–80. <https://doi.org/10.1016/j.coldregions.2015.02.007>.